This ESI replaces the version published on the 17th of December 2019 which contained an incorrect Fig. S4. The current version was published on the 15th of July 2020.

Supporting Information

A highly reversible Neutral Zinc/Manganese Battery for Stationary Energy Storage

Congxin Xie[1,2], Tianyu Li[1], Congzhi Deng[2], Yang Song[1], Huamin Zhang[1], Xianfeng Li[1]*

[1] Division of Energy Storage, Dalian Institute of Chemical Physics, Chinese Academy of Sciences, 457 Zhongshan Road, Dalian 116023 (P. R. China), Email: lixianfeng@dicp.ac.cn

[2]University of Chinese Academy of Sciences, Beijing 100039 (P. R. China)

* Corresponding author

Materials

Analytical grade $ZnCl_2$ (DAMAO Chemical Reagent Factory, Tianjin, China), $Mn(Ac)_2$ (Sinopharm Chemical Reagent Co.,Ltd), KCl (DAMAO Chemical Reagent Factory, Tianjin, China) and $Zn(Ac)_2$ (Sinopharm Chemical Reagent Co.,Ltd.), $Na_4P_2O_7$ (DAMAO Chemical Reagent Factory, Tianjin, China), graphite felt (Liaoyang J-Carbon Materials Co., Ltd., China), PVDF(Arkema), Super P (TIMCAL), and porous polyolefin membrane (900 μm thickness) were used as received. The Nafion solution and Nafion 115 membrane were purchased from Dupont. All electrolytes were prepared with deionized water.

CV test

The CV test was conducted by a typical three-electrode system on a Gamary electrochemical workstation. A glassy carbon electrode (d=5 mm) was chosen as the working electrode and a graphite plate (5cm*5cm) and a SCE (saturated KCl) electrode were employed as the counter and

reference electrode respectively. For the $Mn(Ac)_2$ electrolyte, 0.05 M $Mn(Ac)_2$ in 1 M KCl was scanned at a potential range of 0~1.2V or 0~1.4 V at a sweeping rate of 10 mV/s. To avoid the Cl_2 evolution at high potential (>1.3V *vs.* SHE), for the $MnSO_4$ electrolyte, 0.05 M $MnSO_4$ in 0.5 M K_2SO_4 was evaluated at a potential range of 0.2~1.8V at the sweeping rate of 10 mV/s. Controlled Potential Coulomtry test was carried out by using the above three-electrodes system as well. Different from the above-mentioned test, a graphite plate (3cm*3cm) was used as the working electrode to increase the quantity of product. 250 μL of 0.1 M $Na_4P_2O_7$ solution with hydrochloric acid was added into the evaluated electrolyte to confirm the existence of Mn^{3+}.

The modification of the graphite felt

A certain amount of carbon black (Super P) and PVDF were added into a proper amount of DMAC (Dimethylacetamide) to form a mixture. Then, the mixture was stirred for 10 hours to disperse the carbon black. Afterward, the prepared slurry was coated on porous graphite felt (the thickness was 5mm) with different mass loading. Then, the prepared graphite felt was dried at 70 ℃ until all the solvent (DMAC) was evaporated. The loading capacity and the other relevant information were shown in the table S1.

Table S1. The relevant parameters of graphite felt modification.

Loading capacity	Super P (g)	DMAC (mL)	PVDF (g)	graphite felt area (cm^2)
2 mg/cm^2	2	600	0.5	1000
12 mg/cm^2	12	600	1.2	1000
16 mg/cm^2	16	600	1.6	1000
20 mg/cm^2	20	600	2	1000

Before battery assembly, the modified electrode was firstly immersed in ethanol for half an hour. Then, the graphite felt was soaked in deioned water for more than 10 hours to remove the ethanol. The graphite felt was used for the positive electrode of the flow battery and static battery.

XRD -diffraction and Raman spectroscopy measurement

The precipitation on the positive electrode was analyzed by X-ray diffraction (PANalytical, X'pert Powder X-ray diffractometer) and Raman Spectroscopic system (Renishaw), Diode-pumped solid-state (532 nm) was employed as the laser source.

Comparison with Zinc Ion batteries

The zinc-ion batteries (ZIB) for comparison were shown in reference below[1-15]. The areal capacity (mAh/cm^2) and power density (mW/cm^2) were calculated as follows.

1. The areal capacity C (mAh/cm^2) was calculated based on the following equation:

$$C= C'*m,$$

where C' was the specific capacity during discharge process (mAh/g), m was the mass loading of the active material (g/cm^2).

2. The calculation process of the power density W (mW/cm^2) was as follows:

$$W=I'*V,\ I'=I*m,$$

I' was the areal current density (mA/cm^2), I was the mass current density (mA/g) , m was the mass loading of the active material (g/cm^2), V was the discharge voltage of the battery (V).

Density function theory (DFT) calculation

Density function theory (DFT) calculations of all the components were carried out using the Gaussian 16[16] suit of program. The structure of all the component was optimized using the Becke[17], Lee and Yang[18] three-parameter hybrid functional (B3LYP) method, with 6-311++(d,p) level of basis set. Then all optimized structures for the above components were checked by vibrational frequency analysis[19] to ensure that they were on the minima of potential energy surface.

The Gibbs free energy of component A was calculated by the following equation:

$$G_A = G_A^{\text{gas}} + \Delta G_A^{Sol.}$$

Where G_A was the Gibbs free energy of component A in the solution condition (298.15 K, 1 atm). G_A^{gas} was the Gibbs free energy of component A in the gas phase (298.15 K, 1 atm) and it was calculated by addition of high-accuracy single point of component A at B2PLYP[20]/def2-TZVP level of calculation and the thermal correction to Gibbs Free Energy A. $\Delta G_A^{Sol.}$ was the Solvation

free energy of component A. The Universal Solvation Model Based on Solute Electron Density (SMD)[21] was used to calculate the free energy of solvation in water and was calculated by following the comment proposed by Junming etal[22] at M052X/6-311++(d,p). Experimental free energy of solvation was used for H_2O ($\Delta G_{water}^{Sol.}$=-26.4 kJ/mol, and addition of 10 kJ/mol RTln (55.6) was added to the H_2O free solvation energy, because the concentration of liquid water is 55.6 M). The Standard potential for a reaction was calculated by following Jorge etal's [23] study.

Battery assembly

The battery was assembled following our previous report[24]. For the positive side, the modified graphite felt (6 cm*8 cm) was chosen as the electrode, while, for the negative side, a pristine graphite felt was employed for the zinc deposition. The battery was terminated by the capacity limit for the charging process and a voltage cutoff of 0.1V for the discharging at a constant current density within the range of 20-80 mA/cm^2. Furthermore, for the long cycling test of Figure 6b and Figure S10a, a deep discharge process (keep the voltage at 0.1 V until the current reach about 10 mA) was employed after the constant discharging at 40 mA/cm^2. For the battery assembled with centrifugal pump, a 50 mL electrolyte was pumped into the positive and negative compartment respectively. As for the Zn-Mn static battery, it could be assembled by removing the pumps and pipeline on the positive and negative side. By the way, a piece of Zn-plate (1mm) was placed between the graphite felt and collector for the static battery. As for the peristaltic pump system, 5 mL common electrolyte was pumped to the positive and negative side respectively (Nafion 115 membrane was used to avoid the water crossover). The electrode size was 3cm *3cm. And a zinc plate was used to avoid the accumulation of MnO_2.

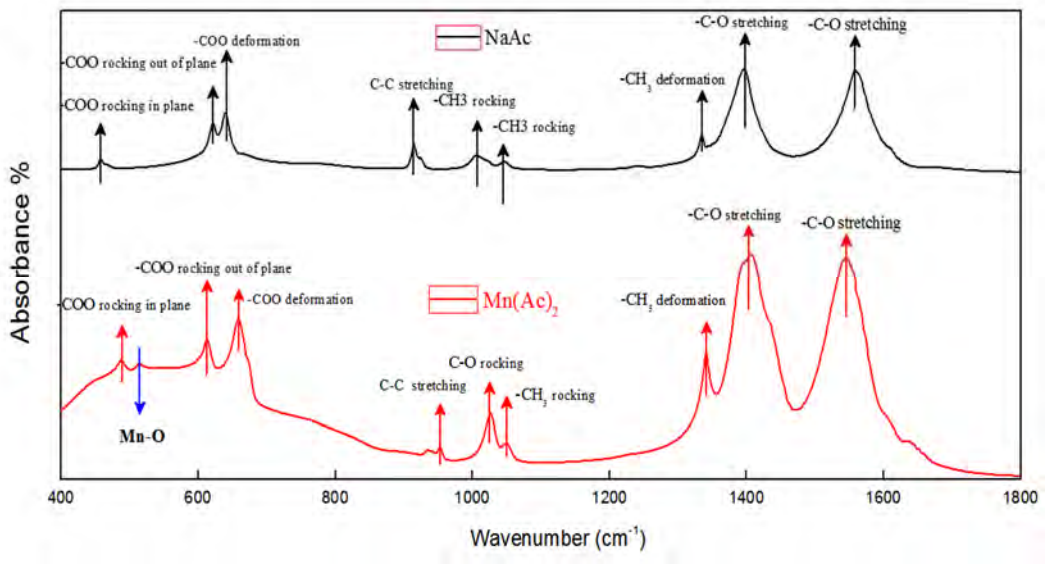

Figure S1. The infrared spectrum of NaAc and $Mn(Ac)_2$.

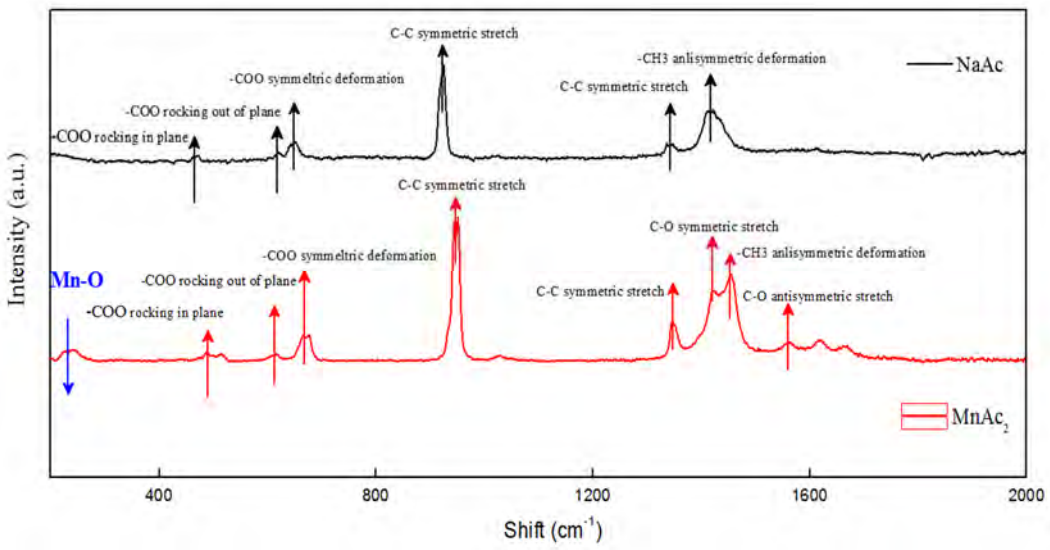

Figure S2. The Raman spectrum of NaAc and $Mn(Ac)_2$.

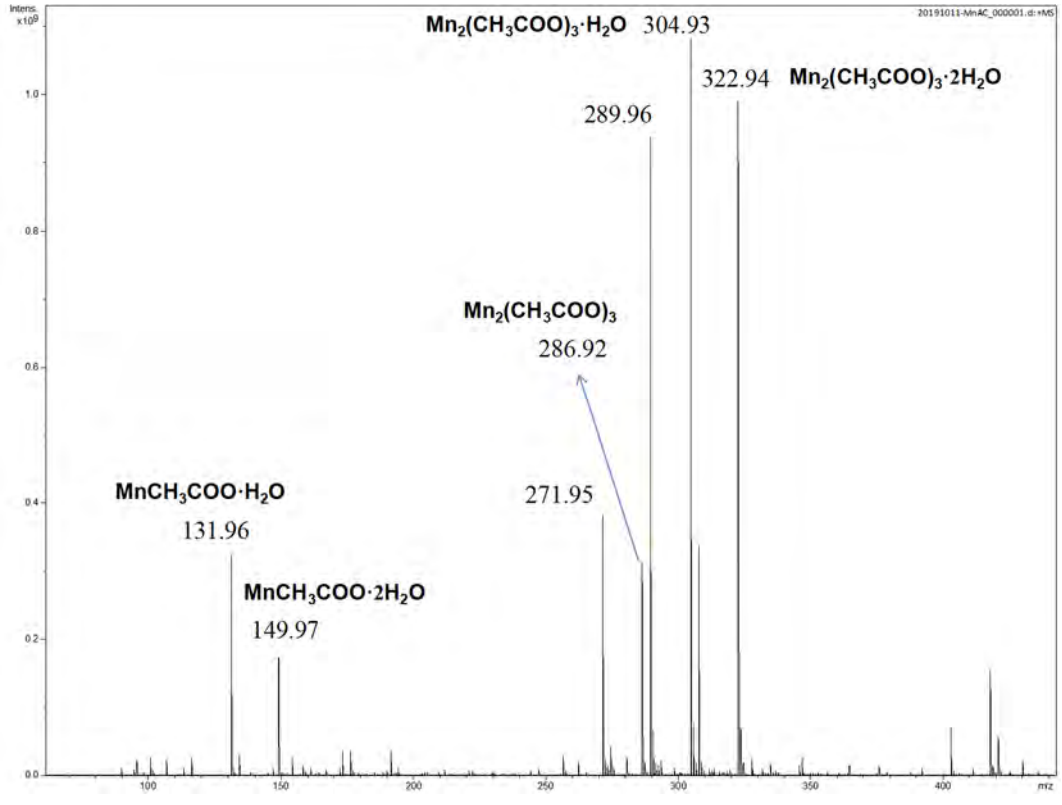

Figure S3. ESI-MS of the $Mn(Ac)_2$ solution.

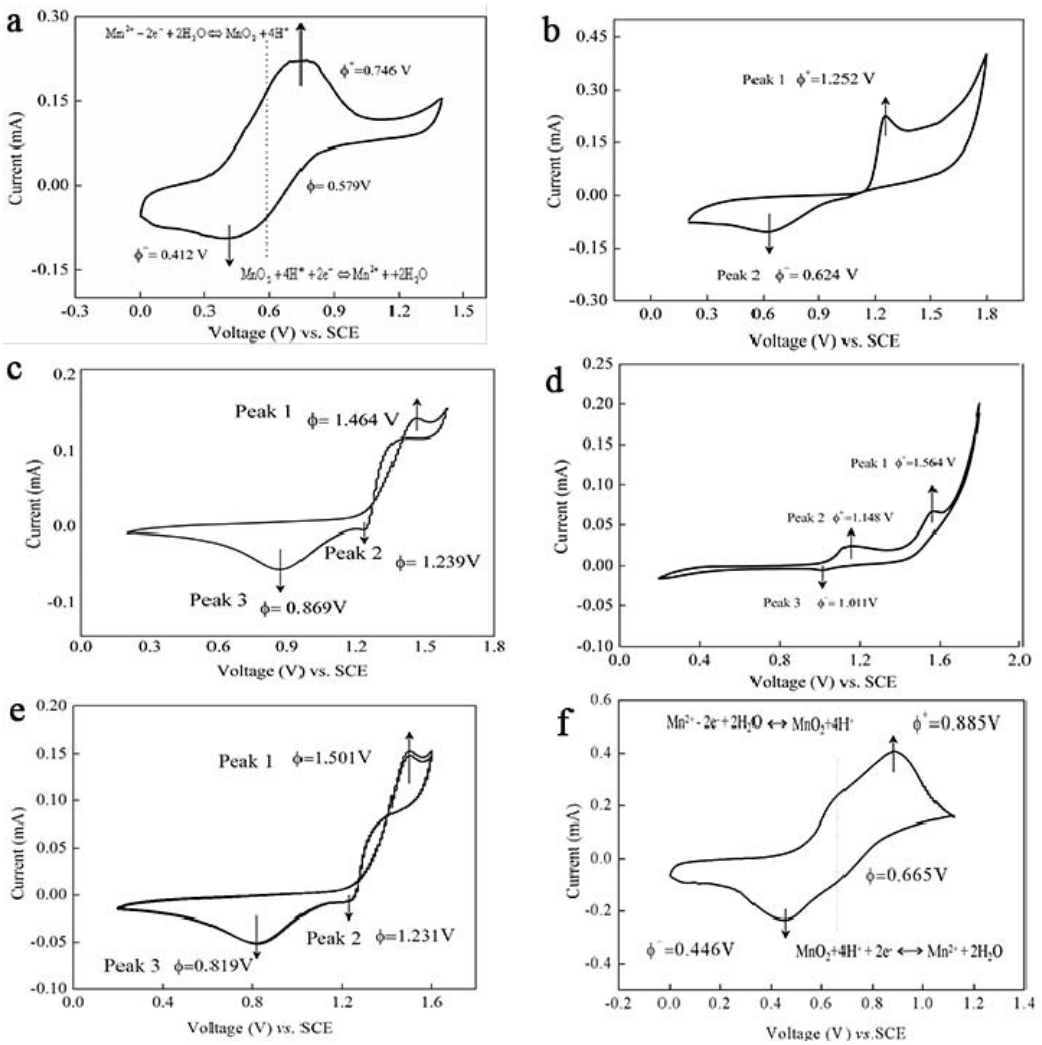

Figure S4. The CV plot of different electrolyte compositions. (a) 0.05M $Mn(Ac)_2$ in 1M KCl at a wider voltage range. (b)The electrochemical behavior of 0.05M $Mn(Ac)_2$+2M KCl+0.1M H_2SO_4 solution. (c) 0.05 M $Mn(Ac)_2$ in 3 M H_2SO_4. (d) The electrochemical behavior of 0.05 M $MnSO_4$+0.5M K_2SO_4+ 0.1M H_2SO_4 solution. (e) The 0.05M $MnSO_4$ in 3 M H_2SO_4. (f) 0.05 M $MnSO_4$ and 0.1M KAc in 0.5M K_2SO_4.

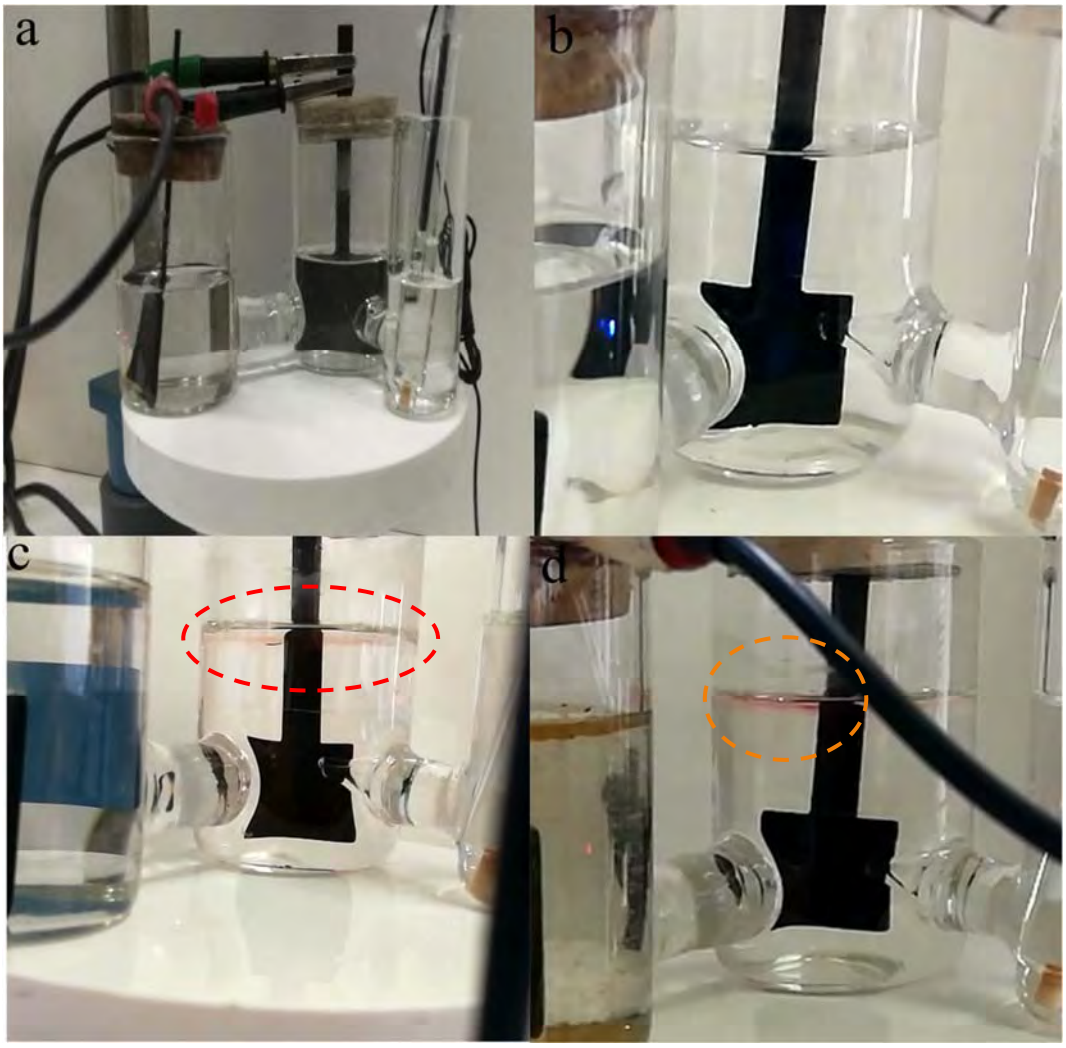

Figure S5. The optical images of different electrolyte composition after a Controlled Potential Coulomtry test. (a) The illustration of 0.05 M $Mn(Ac)_2$ at 0.78 V . (b) The photographs of 0.05 M MnSO4 at 1.0 V. (c) 1.3 V (d) and 1.5 V.

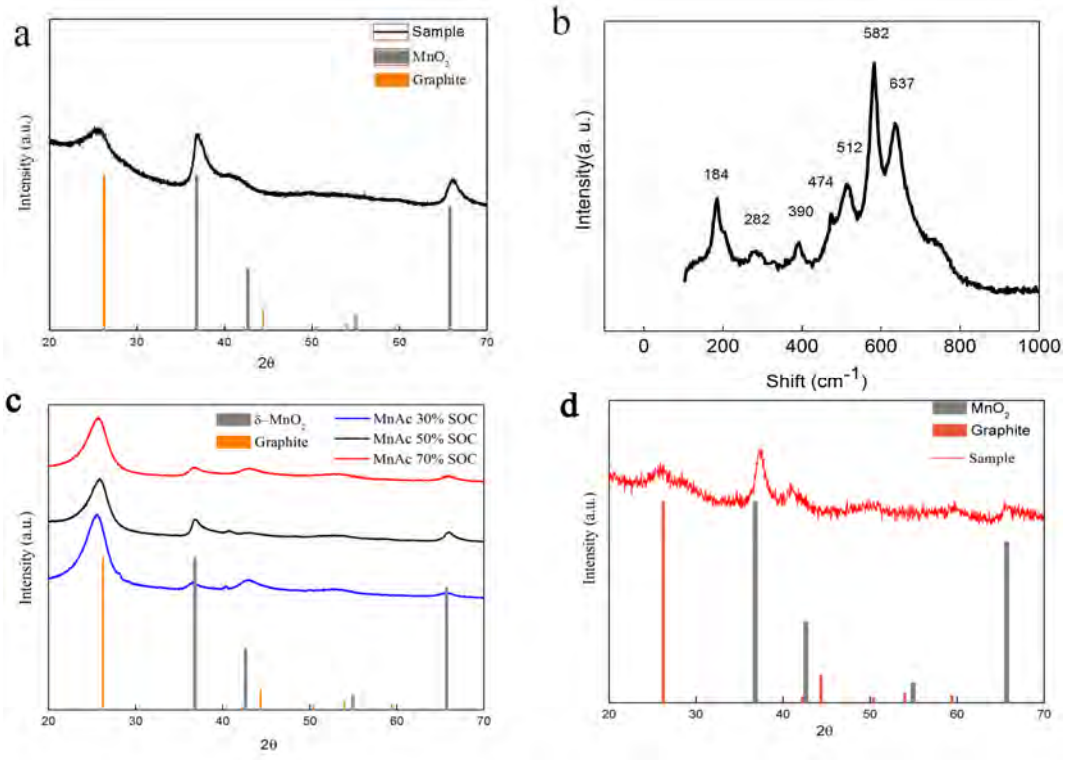

Figure S6. (a) The XRD patterns of the deposition from $Mn(Ac)_2$. (b) Raman spectra of the deposition on the positive electrode. (c)The XRD patterns of the deposition from $Mn(Ac)_2$ at different SOC. (d) The XRD pattern of the deposition under certain discharge state. Electrolyte composition: 0.5M $Mn(Ac)_2$, 0.5M $ZnCl_2$ and 2M KCl.

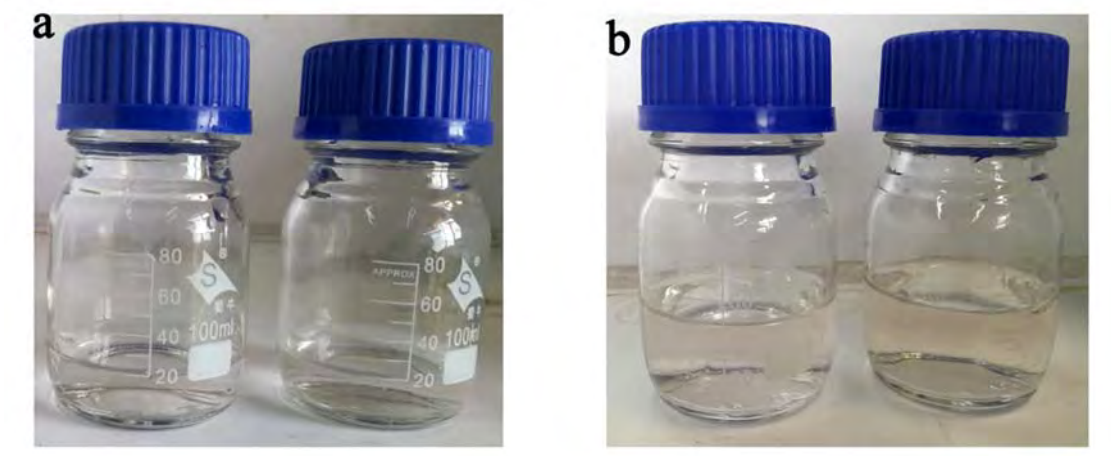

Figure S7. The visualization experiments of the $Mn(Ac)_2$ electrolyte. (a) The phototypes of the partially charged electrolyte added with $Na_4P_2O_7$ solution（the right was the pristine and the left was the contrast with $Na_4P_2O_7$），(b) and a continuous charging to higher SOC（the right was the

pristine and the left was the contrast with $Na_4P_2O_7$）.

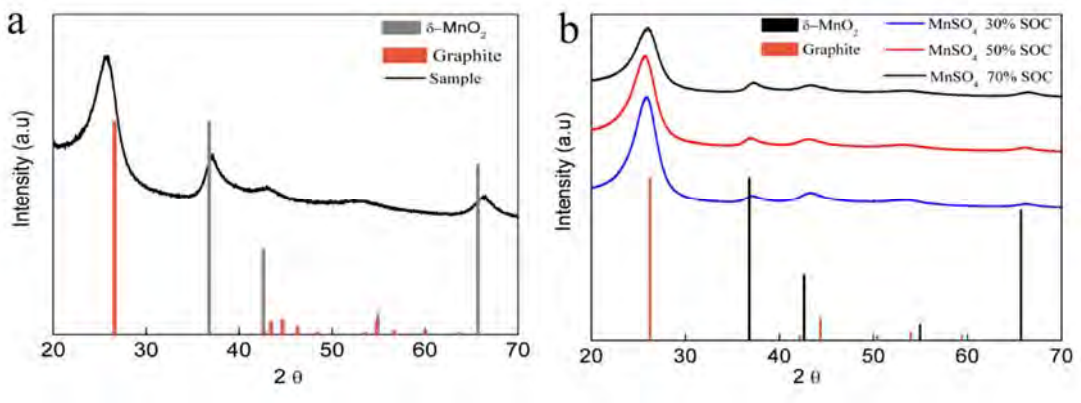

Figure S8. (a) The XRD evaluation of the deposition from $MnSO_4$. (b)The deposition at different SOC. **(**Electrolyte composition 0.2M $MnSO_4$+0.2M $ZnSO_4$+0.5M K_2SO_4.)

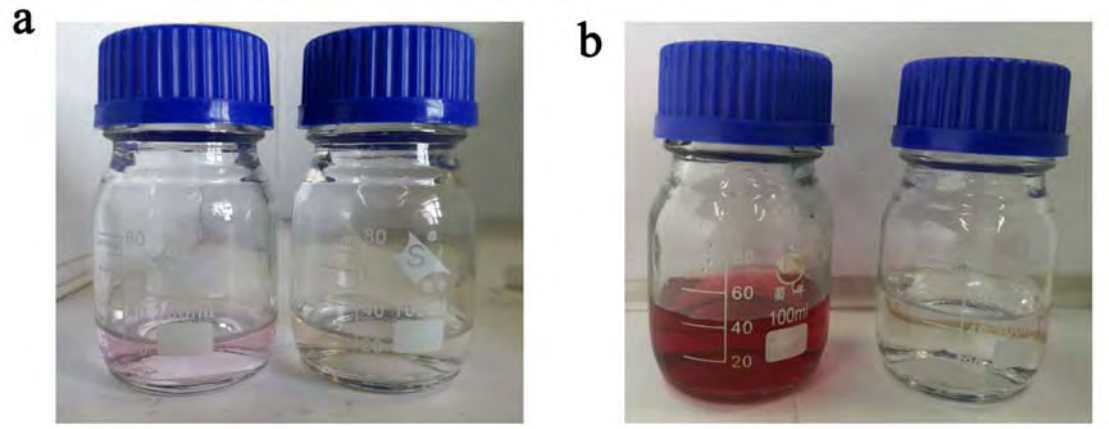

Figure S9. The visualization experiment of $MnSO_4$ based flow battery. (a) Adding $Na_4P_2O_7$ into the partial charged electrolyte. (b) The phototype of "a" after a continuous charging to higher SOC.

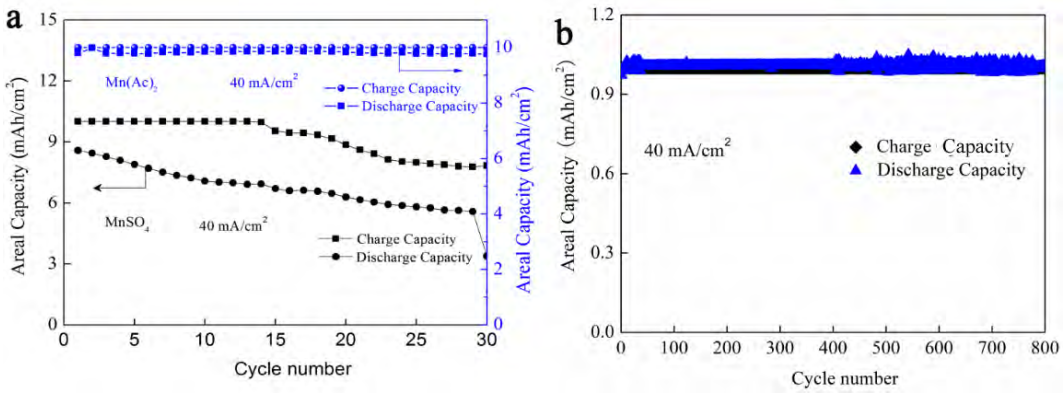

Figure S10. The cycling performance of the $Mn(Ac)_2$ and $MnSO_4$ based batteries. (a) The performance of the battery with the areal capacity 10 mAh/cm^2 and (b)1mAh/cm^2.

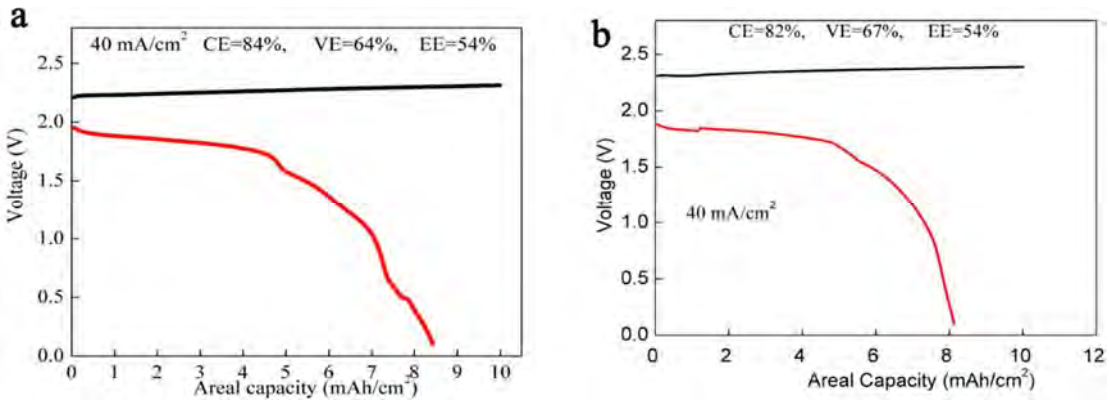

Figure S11. (a) The performance of the battery assembled with 0.2 M $MnSO_4$+0.2 M $ZnSO_4$+0.5 M K_2SO_4 electrolyte. (b) The battery assembled with Zn plate on the negative side and 0.1 M H_2SO_4 was added to the positive tank at the end of charging and then discharging.

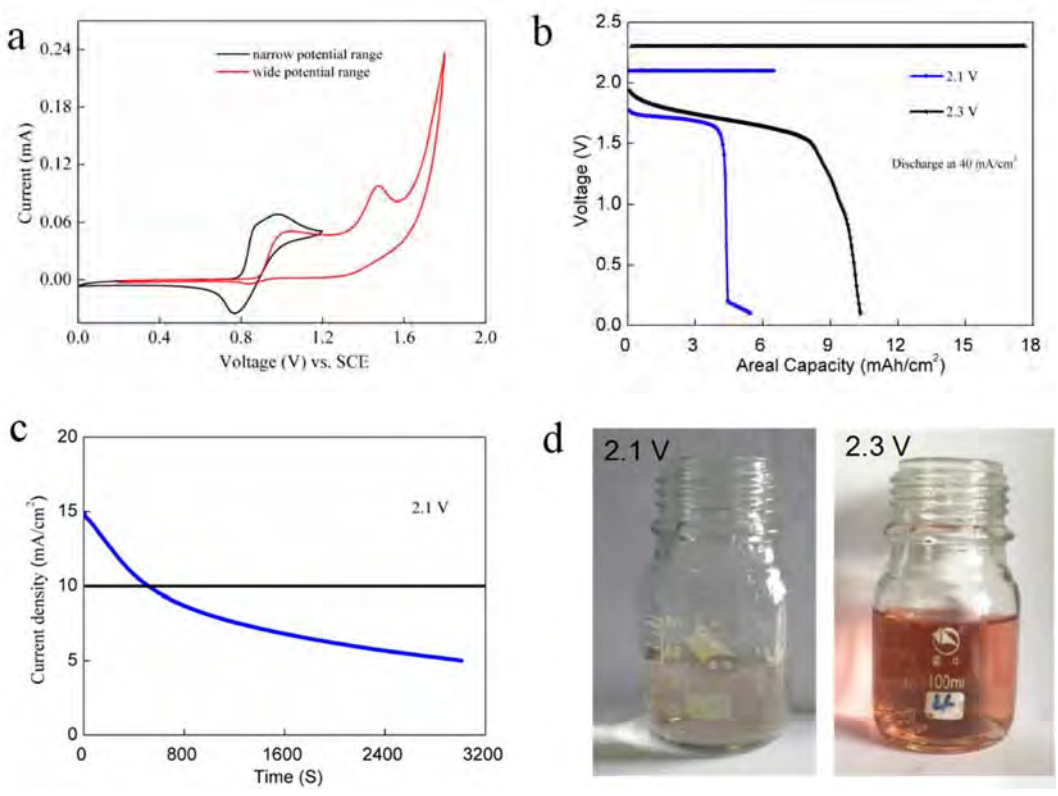

Figure S12. (a) The CV plot of $MnSO_4$ with the different potential range. (b) The charge-discharge curves of $MnSO_4$ system at different potential. (c) The current density versus time at the potential of 2.1 V in "b". (d) The photographs of electrolyte color detection under different charging potentials (Adding $Na_4P_2O_7$ into the partial charged electrolyte).

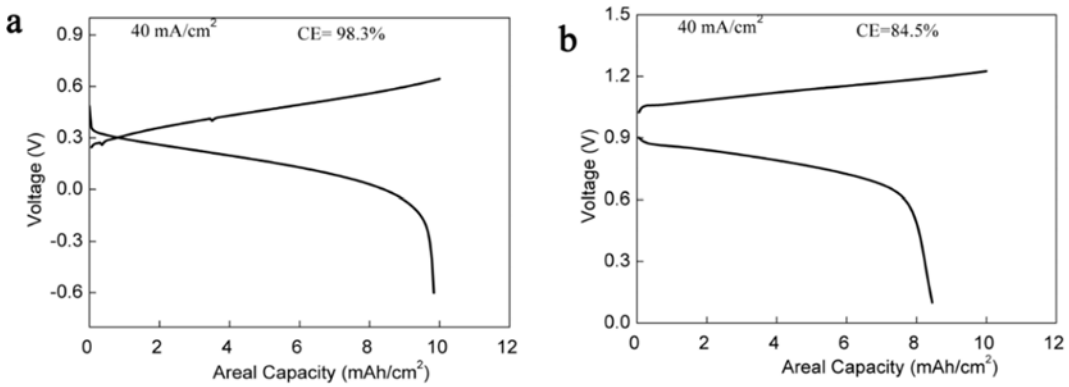
a
40 mA/cm2
CE= 98.3%
Voltage (V)
Areal Capacity (mAh/cm2)
b
40 mA/cm2
CE=84.5%
Voltage (V)
Areal Capacity (mAh/cm2)

Figure S13. (a) The charge-discharge plot of Cu-$Mn(Ac)_2$ system ($Mn(Ac)_2$ was only in the positive side, $CuSO_4$ was only in the negative side; no extra H_2SO_4 was added). (b) The charge-discharge curve of Cu-$MnSO_4$ system ($MnSO_4$ was only in the positive side, $CuSO_4$ was only in the negative side, 0.1 M H_2SO_4 was added to the positive tank at the end of charging).

.

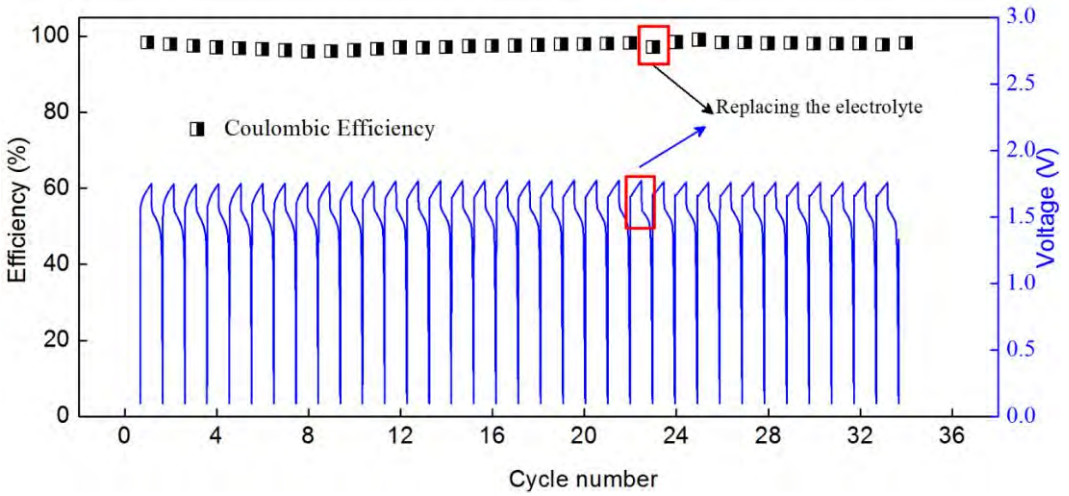

Figure S14. The $Mn(Ac)_2$ based flow battery before and after the positive electrolyte was replaced. (Replacing the electrolyte with fresh of the same PH)

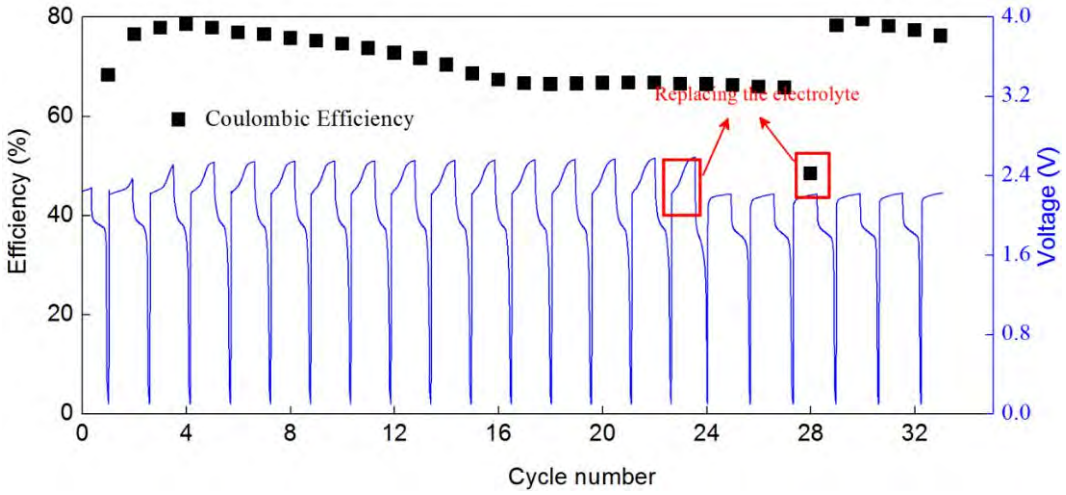

Figure S15. Replacing the positive electrolyte of $MnSO_4$ based flow battery with the fresh (Adjusting to the same PH). The cycling performance and charge-discharge plot of the battery before and after substituting electrolyte.

Figure S16. The photographs of the $MnSO_4$ electrolyte after a long cycling test.

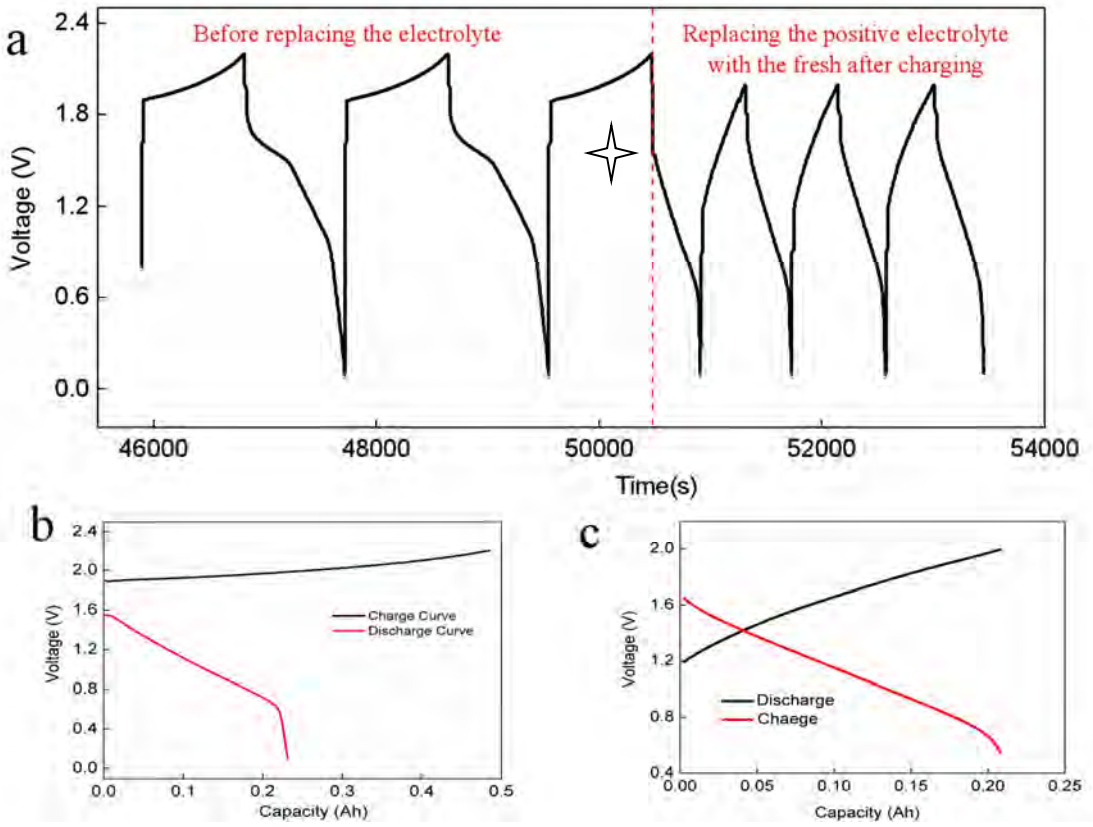

Figure S17. (a)The performance of the battery before and after replacing the positive electrolyte with $ZnCl_2$+KCl. (b) The charge-discharged plot of the marked cycle in "a".(c) The charge-discharge plot after replacing the electrolyte.

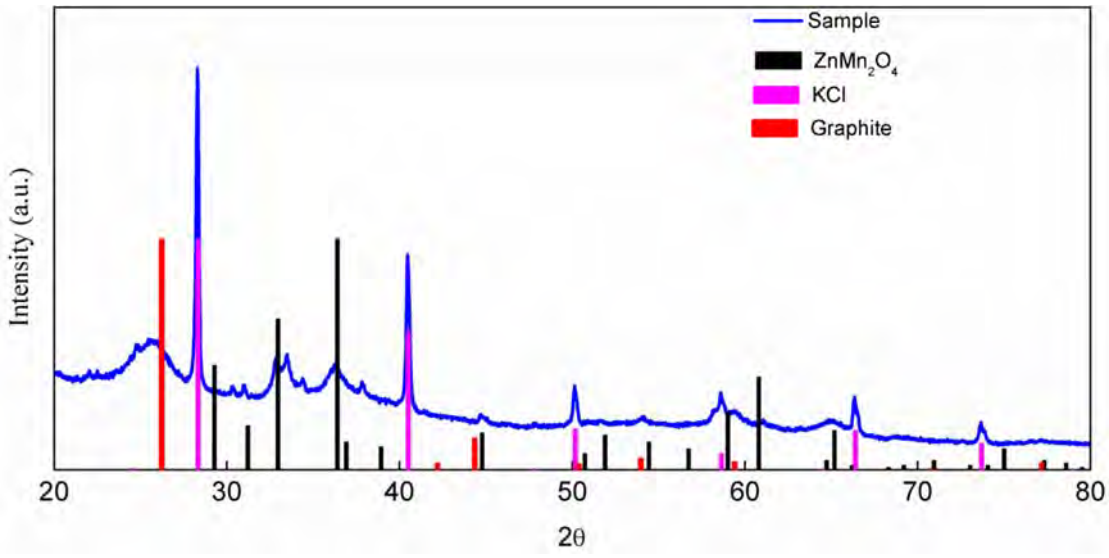

Figure S18. The XRD pattern of the discharge product on the positive electrode after replacing positive electrolyte with $ZnCl_2$+KCl.

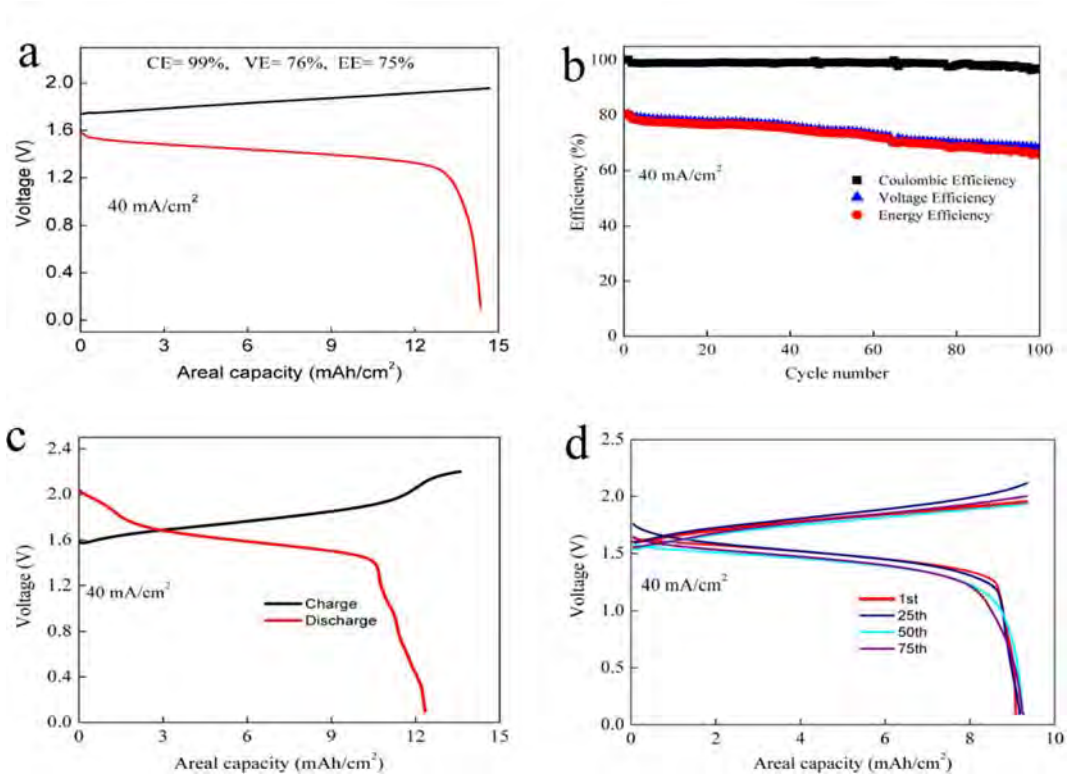

Figure S19. (a) The charge-discharge plot of the battery assembled with 1M $Mn(Ac)_2$+1M $ZnCl_2$+2 M KCl. (b) The coulombic efficiency, voltage efficiency and energy efficiency of the battery assembled with the electrolyte of 1M $Mn(Ac)_2$+1M $ZnCl_2$+2 M KCl at the current density of 40 mA/cm^2. (c) The charge-discharge plot of the battery assembled with the electrolyte of 0.5M $Mn(Ac)_2$+0.5M $ZnCl_2$+2 M KCl at high SOC. (d) The charge-discharge plot of the $Mn(Ac)_2$ based battery for over 100 cycles test (charging time 14 minutes).

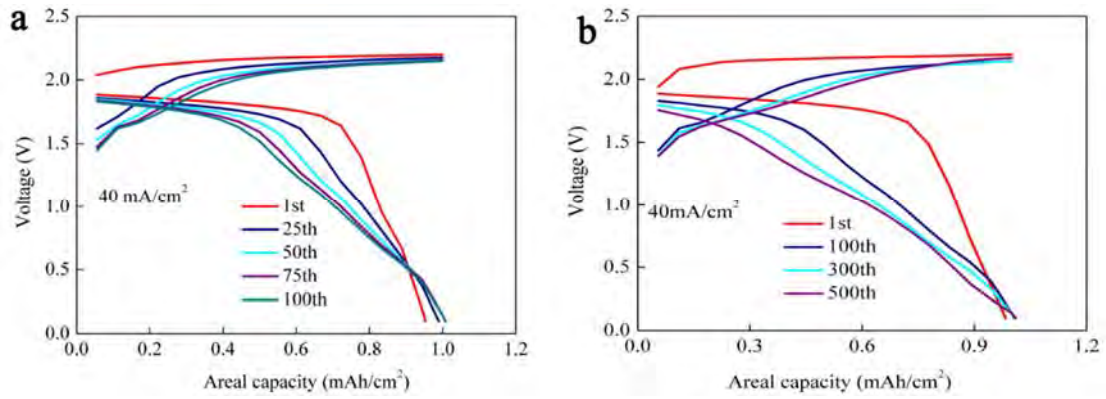

Figure S20. The charge-discharge plot of the Zn-$MnSO_4$ battery in a long cycle test. (a) The charge -discharge plot of the $MnSO_4$ based battery for over 100 cycles test. (b) The plot of the $MnSO_4$ based battery for over 500 cycles cycles test.

Table S2: The Gibbs free energy of all the components in the following equation.

$Mn^{2+}+4HAc+MnO_2+2e^-$--> $2Mn(Ac)_2+2H_2O$ (Equation S1)

$Mn(AC)_2$ (a.u.)	H_2O (a.u.)	Mn^{2+} (a.u.)	HAc (a.u.)	MnO_2 (a.u.)
−1606.7805	−76.3287	−1150.3704	−228.6749	−1300.7614
$2Mn(AC)_2$ (a.u.)	$2H_2O$ (a.u.)	Mn^{2+} (a.u.)	4HAc (a.u.)	MnO_2 (a.u.)
−3213.5611	−152.6574	−1150.3704	−914.6995	−1300.7614

Calculation of the Gibbs free energy of the above Equation:

ΔG= (-3213.5611)+(-152.9098)+1300.7614 + 914.6995 + 1150.3704 = -0.3872（a.u.）

Corrected ΔG=-0.3872*627.509474*4.186-2*1.89= -1020.8597 kJ/mol

The Gibbs free energy for SHE：$H^+ + e^-$ -->1/2 H_2 ΔG=-418 kJ/mol

Therefore, the Voltage for the above reaction versus SHE was:

E= -ΔG/nZF=-(-1020.8597+2*418)*1000/(2*96485)=0.9579 V

Table S3: The Gibbs free energy of all the components in the following equation.

$MnO_2+4H^++2e^-\text{-->}Mn^{2+}+2H_2O$ (Equation S2)

Mn^{2+} (a.u.)	H_2O (a.u.)	H^+ (a.u.)	MnO_2 (a.u.)
−1150. 3704	−76. 3287	-0.4478	−1300. 7614
Mn^{2+} (a.u.)	$2H_2O$ (a.u.)	$4H^+$ (a.u.)	MnO_2 (a.u.)
−1150. 3704	-152.6574	-1.7912	−1300. 7614

Calculation of the Gibbs free energy of the above Equation:

ΔG=(-1150.3704)+(-152.6574)-(-1.7912)-(-1300.7614)=-0.4752 (a.u.)

Corrected ΔG= -0.4752*627.509474*4.186-2*1.89=-1252.01kJ/mol

The Gibbs free energy for SHE：$H^+ + e^- \rightarrow 1/2\ H_2$ ΔG=-418 kJ/mol

Therefore, the Voltage for the above reaction versus SHE was:

E= -ΔG/nZF=-(-1252.01+2*418)*1000/(2*96485)=2.155 V

After calibration: E=2.155 -0.4425=1.7125 V

Based on the table S2 and S3, the potential difference was calculated:

E_{S2}-E_{S1}=1.7125- 0.9579=**0.7546V**

Based on the experiment results, the difference of initial oxidation potential gap between $Mn(Ac)_2$ and $MnSO_4$ was about 0.53 V vs.SHE (0.42 V vs.SCE):

ΔE=0.9-0.37=**0.53V**

Indeed, the difference between the calculated and experiment value is relatively large. The difference between the experiment and calculation is about 0.7 V, which corresponds to 135 kJ/mol of Gibbs free energy. In DFT calculation, the energy differences between different Functional and basis set for a component will up to ~100 kJ/mol according to Jorge etal's[23] study. The Gibbs Free Energy of each components was calculated by $G_A = G_A^{Gas} + \Delta G_A^{Sol.}$. Although G_A^{Gas} was calculated by addition of high-accuracy single point of component A at B2PLYP double hybrid functional at def2-TZVP level of basis set and the thermal correction to Gibbs Free Energy A, there may still be some differences. When calculating $\Delta G_A^{Sol.}$, only the

implicit model based on Solute Electron Density with solution water was taken into consideration, which is a bit different from the experimental circumstances, and then results in such difference.

Reference

1. M. Chamoun, W. R. Brant, C.-W. Tai, G. Karlsson and D. Noréus., *Energy Storage Materials*, 2018, **15**, 351-360.

2. D. Kundu, B. D. Adams, V. Duffort, S. H. Vajargah and L. F. Nazar, *Nat. Energy,* 2016 **1**,16119.

3. Y. Zeng, X. Zhang, Y. Meng, M. Yu, J. Yi, Y. Wu, X. Lu and Y. Tong, *Adv. Mater.*, 2017**,** **29**,1700247.

4. C. Xu, B. Li, H. Du and F. Kang, *Angew. Chem.*, 2012, **51**, 933-935.

5. H. Pan, Y. Shao, P. Yan, Y. Cheng, K. S. Han, Z. Nie, C. Wang, J. Yang, X. Li, P. Bhattacharya, K. T. Mueller and J. Liu, *Nat. Energy*, 2016,**1**, 16039.

6. V. Soundharrajan, B. Sambandam, S. Kim, M. H. Alfaruqi, D. Y. Putro, J. Jo, S. Kim, V. Mathew, Y. K. Sun and J. Kim, *Nano lett.***,** 2018**, 18**, 2402-2410.

7. B. Lee, H. R. Lee, H. Kim, K. Y. Chung, B. W. Cho and S. H. Oh, *Chem. Commun.*, 2015, **51**, 9265-9268.

8. Alfaruqi, M. H. et al., *J. Power Sources*, 2015, **288**, 320-327.

9. C. Xia, J. Guo, Y. Lei, H. Liang, C. Zhao and H. N. Alshareef, *Adv. Mater.*, 2018,**30**, 1705580.

10. N. Zhang, F. Cheng, Y. Liu, Q. Zhao, K. Lei, C. Chen, X. Liu and J. Chen, *J. Am. Chem. Soc.*, 2016, **138**, 12894-12901.

11. Q. Pang, C. Sun, Y. Yu, K. Zhao, Z. Zhang, P. M. Voyles, G. Chen, Y. Wei and X. Wang, *Adv. Energy Mater.*, 2018, **8**, 1800144.

12. P. He, G. Zhang, X. Liao, M. Yan, X. Xu, Q. An, J. Liu and L. Mai, *Adv. Energy Mater.*, 2018, **8**, 1702463.

13. N. Zhang, F. Cheng, J. Liu, L. Wang, X. Long, X. Liu, F. Li and J. Chen, *Nat.Commun.*,2017, **8**, 405.

14. J. Huang, Z. Wang, M. Hou, X. Dong, Y. Liu, Y. Wang and Y. Xia, *Nat. Commun.* 2018, **9**, 2906.

15. W. Chen, G. Li, A. Pei, Y. Li, L. Liao, H. Wang, J. Wan, Z. Liang, G. Chen, H. Zhang, J. Wang and Y. Cui, *Nat. Energy,* 2018, **3**, 428-435.

16. Frisch M J, Trucks G W, Schlegel H B, et al. Gaussian 16 Rev. A.03. Wallingford, CT, 2016.

17. Becke A D, *J. Chem. Phys.*, 1993, **98**, 5648-5652.

18. Lee C T, Yang W T, Parr R G, *Phys. Rev. B* 1988, **37**, 785-789 .

19. Stephens P J, Devlin F J, Chabalowski C F, et al. , *J. Phys. Chem.*, 1994, **98**,11623-11627.

20. Grimme S. *J. Chem. Phys.*, 2006,**124**, 034108.

21. Marenich A V, Cramer C J, Truhlar D G. *J. Phys. Chem. B* ,2009, **113**, 6378-6396.

22. Ho J, Klamt A, Coote M L, *J. Phys. Chem. A*, 2010,**114**,13442-13444.

23. Alí-Torres J, Rodríguez-Santiago L, Sodupe M, et al., *J. Phys. Chem. A*, 2011,**115**, 12523-12530 .

24. Xie, C., Liu, Y., Lu, W., Zhang, H. & Li, X. *Energy Environ. Sci.* **2019**, 12, 1834-1839.